ANISOTROPY IN REACTING COMPRESSIBLE TURBULENT SHEAR FLOW

D. LIVESCU AND C.K. MADNIA
Department of Mechanical and Aerospace Engineering,
State University of New York at Buffalo,
Buffalo, NY 14260

Abstract.

The structure of reacting compressible homogeneous turbulent shear flow is examined via data generated by direct numerical simulations (DNS). The reaction is modeled as one-step, exothermic, irreversible, and Arrhenius type. The effects of reaction are studied by decomposing the velocity field into its solenoidal and dilatational parts. The heat of reaction significantly enhances the dilatational kinetic energy, while it reduces its solenoidal counterpart. The solenoidal and dilatational large scales (kinetic energy) and small scales (viscous dissipation) anisotropies are investigated for cases with different initial turbulent Mach numbers and Reynolds numbers.

1. Introduction

Homogeneous turbulent shear flow represents one of the simplest anisotropic flows and its study can reveal important aspects of the structure and production of the turbulent fluctuations. Moreover, the recent high Reynolds number experiment of incompressible turbulent shear flow of Shen and Warhaft (2000) indicates that the higher order moments of the velocity field are not consistent with the postulate of local isotropy. Although DNS at high Reynolds numbers are not feasible yet, persistent anisotropy of the higher order moments for incompressible shear flow at moderate Reynolds numbers has been observed earlier in the numerical results of Pumir (1996). Compared to incompressible turbulent shear flow, the compressible turbulent shear flow is much less investigated computationally, although the recent studies of Blaisdell, Mansour & Reynolds (1993), Sarkar (1995) and Hamba (1999) have improved our understanding of the influence of compressibility on the structure and development of the flow. The heat release influence on the turbulent shear flow development has been studied by Livescu, Jaberi & Madnia (2001) (hereinafter, referred to as LJM01). However, the reacting flows usually involve a large amount of heat release and thus are intimately related to the compressibility of the flow. Furthermore, the combined effects of heat release and compressibility

on the structure of the turbulent shear flow have not been studied. The main objective of this study is to examine the influence of heat release and compressibility on the large scale and small scale anisotropies in reacting compressible homogeneous turbulent shear flow.

2. Numerical Methodology and DNS Parameters

In order to assess the coupled influence of compressibility and heat release on the structure of the reacting compressible shear flow, DNS of homogeneous sheared turbulence are performed under reacting (heat-releasing) and nonreacting conditions. The continuity, momentum, energy and species mass fractions transport equations are solved using the spectral collocation method. The coordinate system is moving with the mean velocity which makes necessary a periodic remeshing of the grid in order to avoid errors associated with highly skewed grids. The remeshing procedure is carried out in wavenumber space with explicit removal of the modes affected by aliasing. The aliasing errors associated with the evaluation of the nonlinear terms are controlled by using the skew-symmetric form of the convective terms. In the reacting cases, the chemical reaction is modeled by a single step, exothermic, irreversible, Arrhenius-type reaction. The viscosity varies with the temperature according with a power law and $Le = 1$ in all cases.

The velocity fluctuations are initialized as a random solenoidal, 3-D field with Gaussian spectral density function (with the peak at $k_{0v} = 10$) and unity rms. The initial pressure fluctuations are evaluated from a Poisson equation (except for case 3 for which they are set to zero) and the initial density field has the mean value equal to 1 and no fluctuations. For the reacting cases the scalar fields are initialized as "random blobs", with double-delta PDFs (Overholt & Pope, 1996). Details can be found in LJM01. The variables are time advanced in physical space using a second order accurate Adams-Bashforth scheme. The code developed for this work is based on a fully parallel algorithm and uses the standard Message Passing Interface (MPI).

The cases considered in this study, summarized in table 1, have different values for the initial turbulent Mach number, M_{t_0}, and initial Reynolds number, Re_{λ_0}. All cases have the same value of the mean shear rate $S = \partial\tilde{u}_1/\partial x_2 = 5.1$ ($\tilde{u}_i$ is the mass average of the velocity), which is in the range dominated by nonlinear effects. For each case two simulations, nonreacting and reacting, are performed. All reacting cases have the values of the heat release parameter $Ce = 1.44$, computational Damköhler number $Da = 1100$, and Zeldovich number $Ze = 8$. For an initial mean temperature in the range of temperatures prior to ignition in an IC engine, the values for the pre-exponential constant of reaction K_f, the activation energy E_a, and the heat of reaction $-H^0$, are calculated and they are in the range of values for the elementary reactions for hydrocarbon combustion.

The range of Mach numbers considered extends from the nearly incompressible case 1 to the high Mach number case 3 which is at the upper limit for the numerical method considered. The range of Re_{λ_0} extends to values higher than any considered in previous studies of compressible homogeneous turbulent shear flow. The simulations were monitored to ensure that the integral scales remain much smaller than the box size, all scales of motion are fully resolved and no significant shocklet regions develop. Thus, all simulations were stopped between $St = 18$ and 20, except the nonreacting and reacting case 5 which were stopped at $St = 10.5$

Case #	M_{t_0}	Re_{λ_0}	Grid size
1	0.1	21	128^3
2	0.3	21	128^3
3	0.6	21	128^3
4	0.3	14	64^3
5	0.3	50	256^3
2^+	0.3	21	128^3
5^+	0.3	50	256^3

TABLE 1. Parameters for the DNS cases. $^+$ In these cases S is set to zero at $St = 4$.

and $St = 12.5$, respectively, before strong shocklets can be formed in the flow. Cases with different values of the reaction parameters and mean shear rate have also been examined. Although the results for these cases are not shown here, they agree qualitatively with the results presented in this paper.

3. Results

Due to the presence of the mean velocity gradient, the velocity field, initially isotropic, develops to become anisotropic with $K_1 > K_3 > K_2$, where K_1 is the kinetic energy in the direction of the mean velocity (the only component of the kinetic energy with a production term in its transport equation) and K_2 is the kinetic energy in the direction of the shear. In order to examine quantitatively the degree of anisotropy among the kinetic energy components, the Reynolds stress anisotropy tensor is considered:

$$b_{ij} = \frac{< \rho u_i'' u_j'' >}{< \rho u_k'' u_k'' >} - \frac{1}{3}\delta_{ij} \tag{1}$$

In agreement with the previous nonreacting simulations (Sarkar 1995; Hamba 1999) our results show that the anisotropy among the normal stresses increases with increasing M_{t_0}. However, as figure 1 shows, for the reacting cases the normal stresses anisotropy decreases during the time when the reaction is important ($3 < St < 8$). Similar results are also obtained for reacting mixing layers (Luo 1999). For the case of reacting homogeneous shear flow, it is shown in LJM01 that this decrease can be associated with two effects, a decrease in the solenoidal kinetic energy in the direction of the mean velocity due an enhanced viscous dissipation and an increase in the dilatational part of the kinetic energy in the direction of the mean shear. However, after the reaction is completed ($St > 10$) the normal stresses anisotropy becomes larger than in the nonreacting case. This behavior is related to reduced levels of the pressure strain terms, responsible for the energy redistribution among the kinetic energy components. As the value of the shear rate S is set to zero, the flow starts to return to isotropy (figure 1), although some small persistent anisotropy can be observed for the time range examined.

As explained by LJM01, the solenoidal and dilatational parts of the kinetic energy are influenced differently by the reaction. Therefore, in order to understand the heat release effects, it is more useful to study separately the anisotropy among the dilatational and solenoidal components of the normal Reynolds stresses. We define a measure of the anisotropy of the normal stresses as:

$$a_K^\alpha = \left[(b_{11}^\alpha)^2 + (b_{22}^\alpha)^2 + (b_{33}^\alpha)^2\right]^{1/2} \tag{2}$$

where $b_{ij}^\alpha = < \rho u_i''^\alpha u_j''^\alpha > / < \rho u_k''^\alpha u_k''^\alpha > -1/3\delta_{ij}$, and $\alpha = s$ or d represents the solenoidal or dilatational part, respectively. Helmholtz decomposition is used to split the normal Reynolds stresses into their solenoidal and dilatational components. In the extreme case where $b_{11}^\alpha = 2/3$ and $b_{22}^\alpha = b_{33}^\alpha = -1/3$, $a_K^\alpha = \sqrt{2/3}$ and thus $0 \leq a_K^\alpha \leq \sqrt{2/3}$.

Figure 2 shows that a_K^s increases as M_{t_0} increases, and this can be mainly associated with a decrease in the solenoidal pressure strain terms. For the reacting cases, as shown by LJM01, the heat release influences the solenoidal parts of the normal Reynolds stresses mainly through the viscous terms. Furthermore, the increase in the solenoidal viscous dissipation components is such that the anisotropy among the solenoidal parts of the normal stresses is little affected. As a result, as figure 2 shows, the values of a_K^s for the reacting and nonreacting cases are close during the time when the reaction is important. At later times a_K^s becomes larger for the reacting cases compared to the nonreacting cases, although the difference between the values obtained for the reacting and nonreacting cases decreases with increasing Mach number.

The influence of the initial value of the Reynolds number on the evolution of a_K^s is presented in figure 3(a). As expected, a_K^s decreases with increasing Re_{λ_0} for both nonreacting and reacting cases. After S is set to zero, a_K^s decreases initially, then reaches a quasi-steady state. This persistent (although small) anisotropy decreases with increasing Re_{λ_0} and it is discussed in more detail below.

It is found in LJM01 that the explicit dilatational effects occur predominantly in the direction of the mean velocity gradient in both nonreacting and reacting cases. The role of the reaction is to significantly amplify these effects, during the time when the reaction is important. Consequently, as figure 3(b) shows, the anisotropy among the dilatational components of the normal Reynolds stresses increases by the reaction. By comparing the results presented in figures 3(a) and (b) it can be seen that the anisotropy levels remain higher for a_K^d than for a_K^s after S is set to zero. For clarity, the results obtained for the reacting cases 2^+ and 5^+ are not shown in figure 3(b) but they are consistent with the discussion above. The M_{t_0} influence on the evolution of a_K^d has also been examined but no clear trend has been observed, although it seems that the behavior at small and large values of M_{t_0} is different.

The quantity a_K^α is defined based on the kinetic energy components and thus it can be associated with the anisotropy at large scales. The small scale anisotropy has been studied in detail for incompressible flows for a large range of Re_λ and it is generally agreed that the second order moments are consistent with the requirements of local isotropy postulate (Saddoughi & Veeravalli 1994; Shen & Warhaft 2000; Ferchichi & Tavoularis 2000). Much less is known, however, about the small scale anisotropy in compressible flows or the differences between the small scale behavior of the solenoidal and dilatational velocity fields. Although the values of the Reynolds numbers in the present study are not high enough to address the

issues of the local isotropy postulate, our results can be useful for modeling purposes and to shed some light on the physics of the solenoidal and dilatational fields in turbulent reacting flows.

Consistent with the definitions for the viscous dissipation terms in the transport equations for the solenoidal and dilatational parts of the normal Reynolds stresses provided in LJM01, the measures of the anisotropies of the solenoidal and dilatational dissipations are defined as:

$$a_\epsilon^\alpha = \left[(d_{11}^\alpha)^2 + (d_{22}^\alpha)^2 + (d_{33}^\alpha)^2\right]^{1/2} \tag{3}$$

where $d_{ij}^\alpha = \epsilon_{ij}^\alpha/\epsilon_{kk}^\alpha - 1/3\delta_{ij}$, and ϵ_{ij}^s and ϵ_{ij}^d are the components of the solenoidal and dilatational viscous dissipation tensors, respectively. Figure 4 shows that the solenoidal dissipation anisotropy has a similar dependence on M_{t_0} as a_K^s, for nonreacting as well as for reacting cases. The difference between the late time values of a_K^s and a_ϵ^s for the reacting and nonreacting cases decreases at higher values of M_{t_0}. In order to examine which scales of motion are responsible for this behavior, the three-dimensional power spectra of the solenoidal velocity are examined in figure 5 at $St = 18$. It can be seen that the energy levels are lower at all scales at higher M_{t_0} for both nonreacting and reacting cases. However, for the reacting cases the small and intermediate scales are mostly affected. Since the small scales are more isotropic, the energy decrease at small scales for the reacting cases can be associated with an increase in the anisotropy of the flow. Moreover, for the reacting cases the small scales energy levels decrease more at lower M_{t_0}. As the Reynolds number increases, a_ϵ^s decreases (figure 6a). However, it remains larger for the reacting cases than for the nonreacting cases. For the highest Re_{λ_0} examined, a_ϵ^s becomes very small after S is set to zero.

The dilatational dissipation anisotropy becomes larger than its solenoidal counterpart after the initial development time for both reacting and nonreacting cases (figure 6b). Unlike a_ϵ^s, a_ϵ^d is much larger for the reacting cases than for the corresponding nonreacting cases during the time when the reaction is important, which is consistent with the discussion above about the amplification of the dilatational effects by the reaction in the direction of the mean velocity gradient. After the mean shear rate is set to zero, even for the case with the highest Re_{λ_0} examined, there are still some persistent anisotropy levels. For clarity, the results obtained for the reacting cases 2^+ and 5^+ are not shown in figure 6(b) but they are consistent with the discussion above.

For reacting decaying isotropic turbulence, Jaberi, Livescu & Madnia (2000) show that the heat release increases the dilatational kinetic energy, unlike the solenoidal energy, at all scales. Figure 7 shows that at $St = 6$, which is close to the time when the mean reaction rate peaks for case 5, the dilatational energy is enhanced at all scales by the reaction. As the reaction is completing ($St > 10$), the contributions from the production and pressure dilatation terms to the increase in the dilatational kinetic energy decrease (LJM01). Moreover, due to the higher temperature, the viscous dissipative effects are still significant and the energy in the small dilatational scales becomes less than in the nonreacting case.

In order to understand the persistent anisotropy levels observed in the normal Reynolds stresses after setting S to zero, the three-dimensional power spectra of the solenoidal and dilatational velocities for the nonreacting case 5^+ at different times are examined in figure 8. It can be seen that the solenoidal kinetic energy is affected mostly at intermediate scales after the shear rate is set to zero. Thus

the largest eddies, which are more anisotropic, are little affected during the initial transient time when the flow adapts to the new conditions. However, the intermediate dilatational scales do not decrease their energy during initial transient time after setting $S = 0$, and the largest scales even increase their energy levels. Therefore, it is expected that some persistent dilatational anisotropy levels should remain in the flow after setting $S = 0$. Although these levels are likely to vanish as the Reynolds number increases, it is important to note that they are larger than for the solenoidal motions, suggesting that the return to isotropy could be different for the solenoidal and dilatational fields.

4. Concluding remarks

DNS are conducted of compressible homogeneous turbulent shear flow under reacting (heat releasing) and nonreacting conditions to examine the coupled influence of compressibility and heat release on the structure of the flow. For the reacting cases the chemical reaction is modeled as one step, irreversible, and Arrhenius type. The parameters considered for this study are the initial values of the turbulent Mach number and the Reynolds number. In order to examine the return to isotropy, after significant anisotropy levels are developed in the flow, the value of the mean shear rate is set to zero for cases with different values of Re_{λ_0}.

In order to study the changes in the structure of the flow due to the heat of reaction and compressibility, the velocity field is decomposed into solenoidal and dilatational parts using the Helmholtz decomposition. Anisotropy tensors are defined for each part of the normal Reynolds stresses and also for the solenoidal and dilatational parts of the viscous dissipation. The results show that both the large and small scale anisotropies are affected by compressibility and heat release. However, the small solenoidal scales tend to be more isotropic than their dilatational counterparts for the range of Reynolds numbers examined. This tendency is also maintained after setting the shear rate to zero.

Acknowledgments

This work is sponsored by the American Chemical Society under Grant 35064-AC9. Computational resources were provided by the San Diego Supercomputer Center, National Center for Supercomputer Applications at the University of Illinois Urbana-Champaign, and the Center for Computational Research at the State University of New York at Buffalo.

References

Blaisdell, G. A., Mansour, N. N. & Reynolds, W. C. 1993 Compressibility effects on the growth and structure of homogeneous turbulent shear flows. *J. Fluid Mech.* **256**, 443-485.

Ferchichi, M. & Tavoularis, S. 2000 Reynolds number effects on the fine structure of uniformly sheared turbulence. *Phys. Fluids* **12**, 2942-2953.

Hamba, F. 1999 Effects of pressure fluctuations on turbulence growth in compressible shear flow. Phys. Fluids **11**, 1623-1635.

Jaberi, F. A., Livescu, D. & Madnia, C. K. 2000 Characteristics of chemically reacting compressible homogeneous turbulence. *Physics of Fluids* **12**, 1189-1209.

Livescu, D., Jaberi, F. A. & Madnia, C. K. 2001 Heat release effects on the energy exchange in turbulent reacting shear flow. Accepted for publication in *J. Fluid Mech.*

Luo, K. H. 1999 Combustion effects on turbulence in a partially premixed supersonic diffusion flame. *Combust. Flame* **119**, 417-435.

Pumir, A. 1996 Turbulence in homogeneous shear flow. *Phys. Fluids* **8**, 3112-3127.

Shen, X. & Warhaft, Z. 2000 The anisotropy of the small scale structure in high Reynolds number ($R_\lambda \approx 1000$) turbulent shear flow. *Phys. Fluids* **12**, 2976-2989.

Saddoughi, S. G. & Veeravalli, S. V. 1994 Local isotropy in turbulent boundary layers at high Reynolds number. *J. Fluid Mech.* **268**, 333-372.

Sarkar, S. 1995 The stabilizing effect of compressibility in turbulent shear flows. *J. Fluid Mech.* **282**, 163-186.

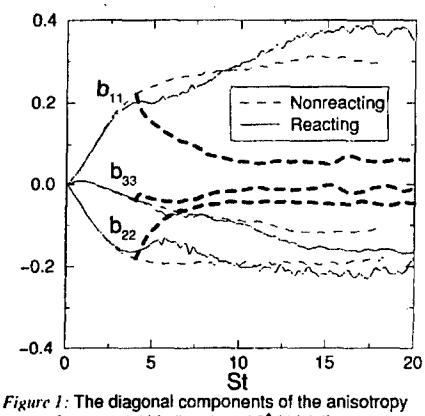

Figure 1: The diagonal components of the anisotropy tensor for case 2 (thin lines) and 2* (thick lines).

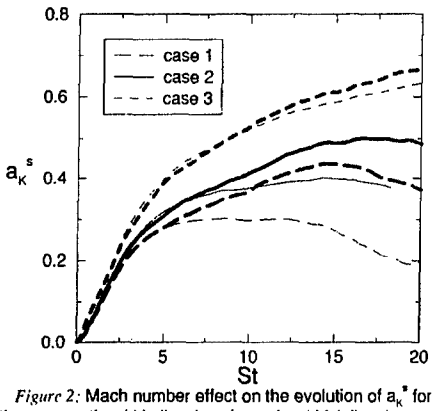

Figure 2: Mach number effect on the evolution of a_K^s for the nonreacting (thin lines) and reacting (thick lines) cases.

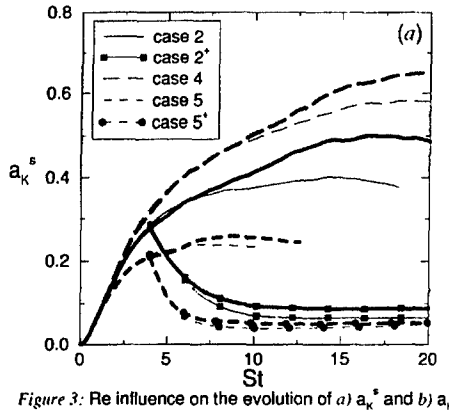

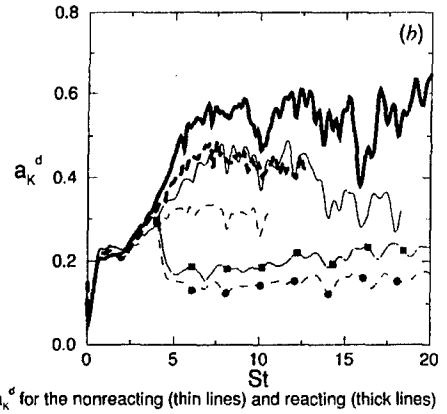

Figure 3: Re influence on the evolution of *a)* a_K^s and *b)* a_K^d for the nonreacting (thin lines) and reacting (thick lines) cases.

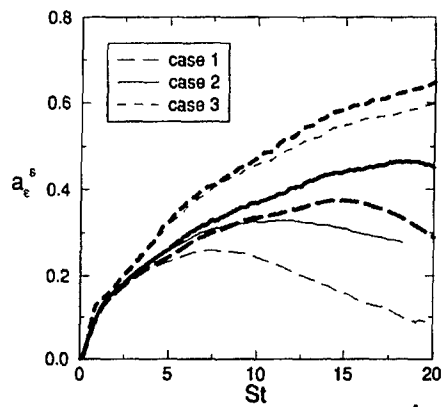

Figure 4: Mach number effect on the evolution of a_ϵ^s for the nonreacting (thin lines) and reacting (thick lines) cases.

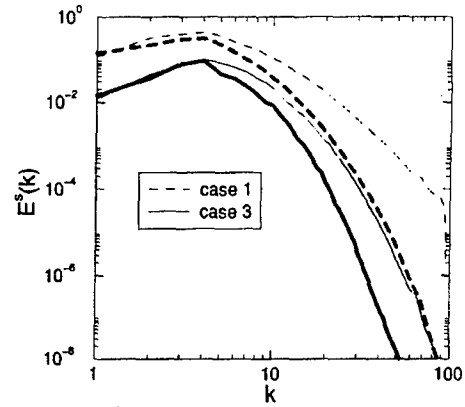

Figure 5: Solenoidal velocity power spectra at St=18 for the nonreacting (thin lines) and reacting (thick lines) cases.

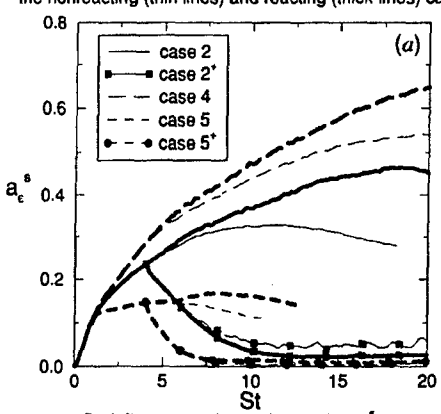

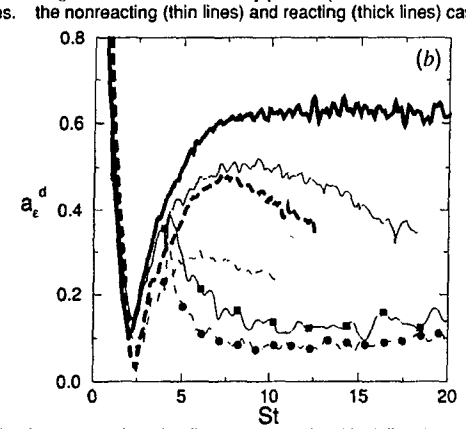

Figure 6: Re influence on the evolution of *a)* a_ϵ^s and *b)* a_ϵ^d for the nonreacting (thin lines) and reacting (thick lines) cases.

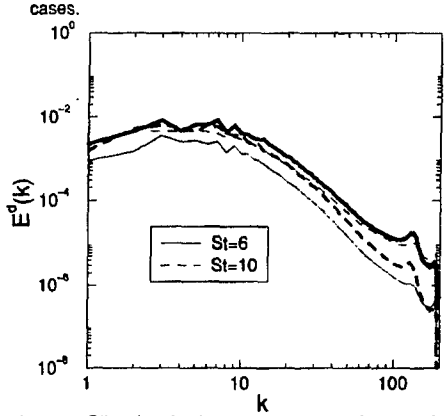

Figure 7: Dilatational velocity power spectra for case 5 nonreacting (thin lines) and reacting (thick lines).

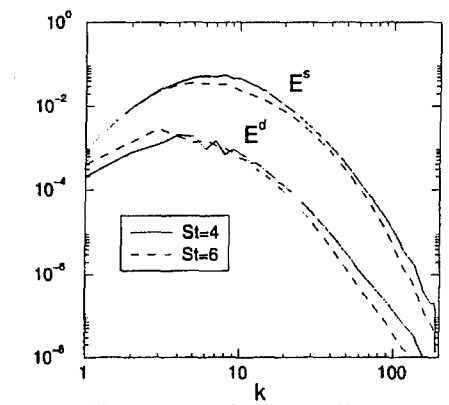

Figure 8: Dilatational and solenoidal velocities power spectra for case 5*.